Finite element assessment of crack initiation and out-of-phase effect on the material behaviour under contact mechanics

Mohammad Almajali
Department of Defense and Security, Rabdan Academy, Abu Dhabi, United Arab Emirates
Omar Quran
Department of Mechanical Engineering, Al-Balqa' Applied University, Balqa, Jordan
Aziz Al-Mahadin
Engineering Technology and Science, Higher Colleges of Technology, Dubai, United Arab Emirates, and
Omer Maaith
Department of Civil Engineering, Mutah University, Karak, Jordan

Abstract

Purpose – This study aims to focus on finite element analysis (FEA) utilising the ABAQUS software program to examine the factors affecting the lifespan of titanium alloy materials in contact. FEA will be used to analyse local fretting variables, including stress, strain and displacement. The contact half-width and other variables will be studied under varying contact loads at different load steps to predict fretting fatigue in terms of fatigue life, crack initiation location and crack initiation orientation.

Design/methodology/approach – The input data for this study were gathered from previous experimental studies conducted on a titanium alloy material commonly used in the compressor and turbine sections of aircraft engines. Four phase angles were used to assess the impact of out-of-phase on fretting fatigue behaviour. The parameters necessary to predict material fatigue life and crack initiation were estimated and examined at different steps and under varying contact loads. The commercial software program, ABAQUS, was employed and the model was validated by comparing it with experimental results, analytical solution and the Ruiz program.

Findings – The study demonstrated a high level of agreement among the FEA results, the Ruiz program and other experimental studies. This finding indicates a significant 145% increase in fatigue life for the out-of-phase condition compared to the in-phase condition.

Originality/value – The use of numerical methods is crucial for efficiently and cost-effectively predicting such behaviour. The developed FEA is valuable for predicting material life and crack initiation.

Keywords Fatigue life, Contact mechanics, FEA, Crack initiation

Paper type Research paper

Introduction

Contact mechanics is a field of study where deformation occurs in a material when two solid surfaces come into contact dynamically. If this contact results from cyclic stress, small amplitude oscillatory movements are generated, subsequently reducing the fatigue resistance of the material and initiating cracks. Generally, the material failure scenario is as follows: a crack forms at the contact edge by Mode II, where the tensile load is at its highest value. The crack then propagates towards the maximum shear stress at ±45°. Upon reaching a critical length, it turns perpendicular to the surface, yielding the maximum Mode I stress intensity. Finally, the cracks propagate rapidly until the material fails. If the material is of low quality and has manufacturing defects, cracks may initiate unexpectedly, consuming the fatigue life of the material during the propagation stage. In contrast, for materials intended for high-tech applications, continuous monitoring of crack initiation is recommended, necessitating the determination and monitoring of stress and the location of early defects in the material. The consequences of such situations include a decrease in the life of the material and an increase in maintenance costs. Thus, manufacturers worldwide have given

The current issue and full text archive of this journal is available on Emerald Insight at: **https://www.emerald.com/insight/1708-5284.htm**

World Journal of Engineering
23/2 (2026) 378–393
Emerald Publishing Limited [ISSN 1708-5284]
[DOI 10.1108/WJE-06-2024-0344]

Received 18 June 2024
Revised 25 July 2024
19 November 2024
Accepted 2 January 2025

significant attention to studying contact mechanism phenomena.

Contact mechanics is demonstrated in detail in (Hills and Nowell, 1994), where several models of the contact mechanics configuration are introduced. One of these models consists of a flat body in contact with a cylindrical body (Figure 1). This model was assumed in the present study. In this model, the flat body was subjected to an axial load σ_{axial}, whereas the cylindrical body was subjected to a normal load, P. The cross-sectional area, thickness and half-thickness of the flat body are denoted by the symbols A, d and b, respectively. The cylindrical end body was assumed to be semi-rectangular, with an arc surface of radius r. When movement begins, a tangential load (Q) is generated. The contact area between the two bodies was identified as 2a, and a was considerably smaller than r. Within the contact area, there were three zones: two slip zones located on both sides and a stick zone is located between them. Essentially, if a material is in contact with another, it will be subjected to both normal and axial loads, and various factors, such as the friction coefficient, environmental conditions, geometry of the components (two bodies), shear stress and applied loads, can affect this contact.

Therefore, numerous studies have been conducted to investigate the effects of various factors and develop appropriate configurations for contact mechanics (Nowell *et al.*, 2006; Dowson *et al.*, 1988; Toshikazu *et al.*, 2004; Lykins *et al.*, 2001; Lee *et al.*, 2003; Sangral and Jayaprakash, 2022). In most of these studies, the friction coefficient was primarily dependent on the applied normal load (Lietch, 2004; Jutte, 2004; Zehsaz and Shahriary, 2013; and Huang *et al.*, 2019). In a recent study, Hintika (Hintikka, 2016) examined contact mechanics with induced frictional behaviour and discovered that the frictional behaviour was controlled by non-Coulomb friction. The material wear behaviour changed as the interface became blocked with wear debris, thereby reducing further wear. (Zhibo *et al.*, 2023) investigated the torsional fretting behaviour of titanium alloy at different parameters. They showed that angular displacement is the most vital factor in dissipated friction energy while the applied normal load can make a difference in friction torque. It has also been reported in many studies (Toshikazu *et al.*, 2004; Lykins *et al.*, 2001; Lee *et al.*, 2003) that the life of a material in contact with another material is considerably reduced compared to its plain fatigue life. For example, (Lee *et al.*, 2003; Jutte, 2004) revealed that as the contact load (P) increases, the fatigue life decreases. (Lee *et al.*, 2003) studied the fatigue life under a variable contact load and observed that the axial stress (σ_{axial}) was the main parameter in determining the material life. A comprehensive review of the effect of cyclic contact loading on fretting fatigue behaviour was presented by (Abbasi *et al.*, 2020). Iyer (Iyer and Mall, 2000) performed fretting fatigue test on titanium alloy at different frequencies; 1 Hz (low-cycle fatigue LCF) and −200 Hz (high-cycle fatigue HCF). HCF is found to curtail the fatigue life regardless of the applied normal load. Additionally, increasing the normal load reduces life at 1 Hz while at 200 Hz, it has no effect. They revealed that the fretting fatigue life is mainly determined by the stress amplitude and high-cyclic frequency of HCF component. The LCF component is found to play a secondary role in the determination of the fretting fatigue life.

(Almajali *et al.*, 2019) Conducted an experimental study on the effect of the phase difference between the contact and axial loads on the fatigue life of titanium alloys. They found that if there is a phase lag between the axial and contact loads, the life of the material increases. In general, the fatigue life of a material subjected to different fatigue situations can decrease from high to low as follows: high cyclic fatigue (HCF), low cyclic fatigue (LCF) with low temperature, high-temperature LCF, and finally, thermal shock (Xin, 2013). Despite numerous experimental studies on contact mechanics, minimal effort has been directed towards numerical studies. Experimental studies are considered expensive in terms of cost and time, particularly

Figure 1 Contact mechanics configuration with a flat body and cylinder body

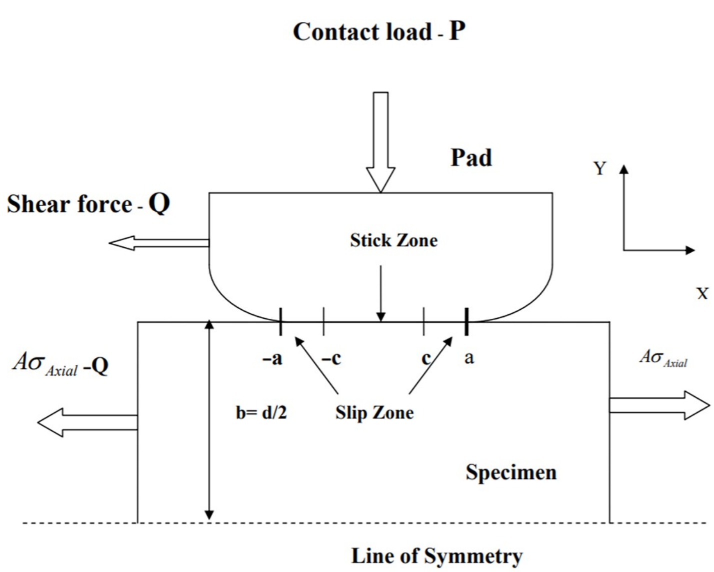

Source(s): Figure by Almajali (2006)

when the induced parameters need to be varied. Thus, it is imperative to develop cheaper and easier techniques to better understand the contact mechanism. To this end, (Chan and Lee, 1988) derived a numerical FORTRAN Ruiz program to compute solutions for related variables, such as stress, strain, peak pressure, and contact half-width (a). Kadiric's numerical study (Kadiric *et al.*, 2003) revealed that the magnitude of the local shear stress increased with an increasing ratio between the root-mean-square roughness and the correlation length. Recently, (Chen *et al.*, 2018) experimentally and numerically studied a dovetail assembly under fretting fatigue behaviour using FEA. Based on the prediction model, they concluded that the entire life of the material was achieved by adding both the life of crack growth and the life of crack initiation. A fixed initial crack length was used, and the predicted results agreed well with experimental results. A new method was developed by (Gonggui *et al.*, 2021) to measure the contact stress of the movable element. They were able to find that the real stress distribution in the rolling or sliding element is alike.

Gailliegue (Gailliegue *et al.*, 2020) investigated the effect of the phase angle between the fretting and fatigue loads on aluminium alloy specimens under four phase angles (0°, 45°, 90° and 135°). He concluded that the phase angle influences the fatigue life of the material and recommended investigating the effects of the phase angle for different materials. On the other hand, Wang (Wang *et al.*, 2023) inspected the influence of loading phase difference (0°, 90° and 180°) on the propagation of the crack for specimen of AA2024-T3. Recently, finite element models have been developed to determine the effect of pad radius on contact parameters (Chaouch *et al.*, 2022). These models were used to describe the impact of various pad radii on contact stresses and damage to crack nucleation. Several studies have recently been conducted to employ a numerical technique to provide a better understanding of the fretting fatigue behaviour of different materials and different applications (Zou *et al.*, 2024; Ahmad *et al.*, 2024; Wang *et al.*, 2023). Xiaohua (Xiaohua *et al.*, 2021) developed a fretting fatigue numerical model of Ti-6Al-4V alloy to determine the crack initiation position and initiation direction and to predict the fatigue life. They used the maximum shear stress criterion and revealed that the predicted fatigue life is in good agreement with the experimental results.

This study aims to incorporate FEA to calculate the local contact mechanism parameters of displacement, stress and strain of titanium alloys. This material is used in many mechanisms subjected to fretting fatigue in the turbine section of aircraft engines. Understanding the behaviour of this material will aid in the development of techniques to decrease the maintenance costs for newly designed components. Finite element analysis was employed in this study to determine local fretting variables, such as stress, strain and displacement. The stress, stress distribution, contact half-width, and other variables were also analysed under variable contact loads at different load steps. In addition, several fretting fatigue parameters, such as the stress range, effective stress, and modified shear stress range, were evaluated for their effectiveness in predicting fretting fatigue in terms of fatigue life, crack initiation location and crack initiation orientation. The commercial software program, ABAQUS, was used for this purpose.

The input data for this study were obtained from Almajlai's experimental studies (Almajali *et al.*, 2019) and (Almajali, 2006), which were conducted on a titanium alloy material used mainly in the compressor and turbine sections of aircraft engines. Four phase angles were used to determine the out-of-phase impact on the fretting fatigue behaviour. The difficulty of using FEA with phase angles arises from the application of loads on different steps. Therefore, the parameters were investigated in different steps and under variable contact loads. Moreover, the main parameters required to predict material fatigue life and crack initiation were estimated, focusing on effective stress, stress range and modified shear stress range (MSSR). (Almajali, 2006) focused on the effect of out-of-phase on the contact mechanics as most of the previous studies have been carried out under a constant applied contact load condition. Additionally, a slight effort has been conducted considering the variable contact load while none has investigated the effect of the phase difference between the axial and the contact loads.

The model was validated by comparing it with the experimental results from (Almajali *et al.*, 2019; Almajali, 2006) the analytical solution, and the Ruiz program. In this case, there is no need to conduct an experimental setup to vary the parameters for the specified material properties and dimensions. Additionally, (Waterhouse and Dutta, 1973) stated that a slight difference in the friction coefficient does not create much deviation in the fretting fatigue parameters, and for titanium alloy, the static friction coefficient ranged between $0.37 \sim 0.46$. Therefore, to simplify the contact analysis in FEA, the coefficient of friction was assumed to be constant with a value of 0.5. This value, which is higher than the largest magnitude of Q/P (Almajali, 2006), was used in all the calculations to obtain a converging numerical solution. It worth mentioning here that ABAQUS software doesn't support time-dependent changes in the friction coefficient. Additionally, it is very critical situation when the friction is changed during the model analysis as sudden change may result in convergence problem.

Finite element analysis

Finite element analysis model

Finite element analysis (FEA) is a simulation method employed to predict the behaviour of the product before manufacturing. FEA can help identify the potential issues with the design and do the essential modifications. This will save time and money, and decrease material failure. FEA can be utilised in various engineering and industrial applications as it allows for enhanced plans and increased safety at early unpredictable levels. It also can accelerate the process by conducting several iterations of the desired prototype. So, FEA indicates how the design will perform practically. In general, FEA is a numerical technique used to calculate the anticipated variables within a contact area. A rigid body is represented as a discrete system comprising several elements that are linked by nodes. The solution to the governing equations of these variables is determined at these nodes. The configuration utilised in this study mirrors that shown in Figure 1. The commercial software program ABAQUS was used to develop the FEA model, as illustrated in Figure 2. In this model, the

Figure 2 Finite element analysis (FEA) model with load and boundary conditions

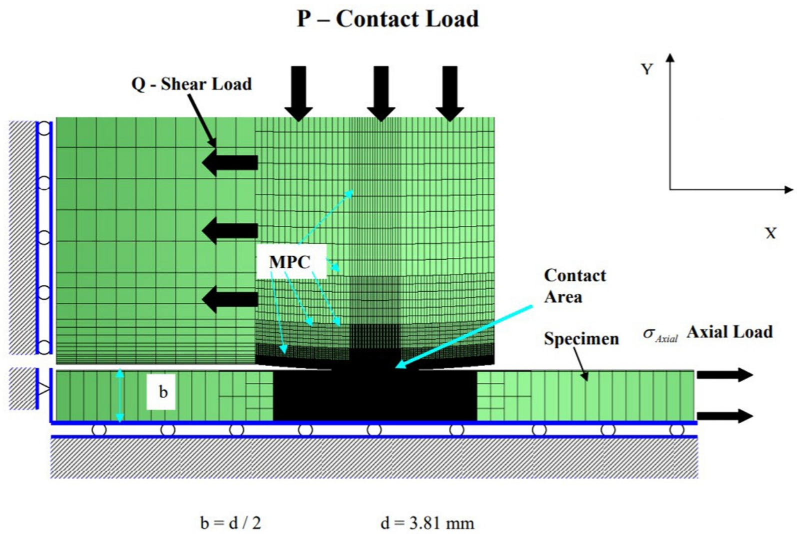

Source(s): Figure by authors

elements are represented by four-node plain-strain quadrilaterals. The primary components of the developed model were the specimen (flat body) and the pad (cylindrical body). To restrict the movement of the pad, an additional rigid body is included in the model. As the model exhibited symmetry about the *x*-axis, only half was used, and it was formulated in two dimensions.

Employing symmetry is one of the most effective methods to reduce the computational time by reducing the total number of degrees of freedom. Specifying the symmetric geometry results in simplifying the associated FEA problem. The nature of the applying loads and the material has to be considered. The symmetry can be employed to model half the specimen only if the rotation at the centre is zero and the displacement is identical. This will reduce the model size and simplify the analysis compared to the full model. Finer mesh can be used to obtain an accurate solution compared to coarse mesh. This does not lead to loss of accuracy as it can be used also if the physical system exhibits symmetry in geometry, loads, constraints, and material properties. In the contact region, nodes from the master surface (pad) and slave surface (specimen) were utilised to create an algorithm for determining load transfer. At the bottom, the specimen is constrained from vertical movement, and it can roll in the x-direction and along the gripped end, whereas it is fixed at the far end in the negative x-direction. On the other hand, the half-space of the specimen was constrained along its boundary in the x and y directions, while the pad was constrained by the holder in the x and y directions. The pad was chosen as the master surface and the specimen was chosen as the slave surface. The nodes on the top side of the pad were forced to move in unison in the y-direction. In the first model, to keep both the pad and specimen from rotating when the loads were applied, a multi-point constraint (MPC) was applied.

In the fretting fatigue condition, the contact region is the critical area where the governing variables must be determined accurately. As meshing process is a concern, four-node plane strain elements are chosen to avoid oscillation along the contact area. Certain geometric coordinates in ABAQUS input file were changed to gradually have more refined mesh towards the centre. The analysis focused on the main variables (stress, strain, and displacement). So, the refinement is vital to include any variation in the values of those variables that could be critical to understand the contact mechanic process. Additionally, it is designed to be a coarse mesh far away from the contact area to save time and memory resources. Both the specimen and pad were made of the same material, namely, a titanium alloy. The material properties were as follows: Young's modulus (E) was 125 GPa and Poisson's ratio (υ) was 0.32. This selection is to ensure that it has a minimum effect on the pads and the specimen to improve the convergence of the FEA. Additionally, it is essential to select an isotropic elasticity material to obtain better accuracy. In this case, the FEA model will help to correlate the stress, strain, and displacement. The dimensions of the model parts were as follows: the half thickness (b) of the specimen was 1.9 mm, and its length was 9.0 mm. The widths of all three parts were the same, measuring 6.3 mm. The contact area is considered to be critical, necessitating the determination of specific parameters. Therefore, the mesh was coarser away from the contact area and refined from the centre of the contact area to optimise the time and memory resources.

Input loads

In FEA, it is crucial to ensure that all the parameters are selected under stable conditions. Therefore, for the FEA input load, data from 10,000 material life cycles were considered, as detailed in previous studies (Almajali *et al.*, 2019; Almajali, 2006). The loads were applied in steps to prevent gross slippage. In addition, Almajali (Almajali *et al.*, 2019; Almajali, 2006) utilised four main phase angles (0° in-phase, 60°, 90° out-of-phase and 105°). Both axial and contact loads, which were variable, were applied in a sinusoidal form. Seven steps were necessary to enter the input data given a constant

Figure 3 Seven steps of load input under the in-phase condition of finite element analysis (FEA)

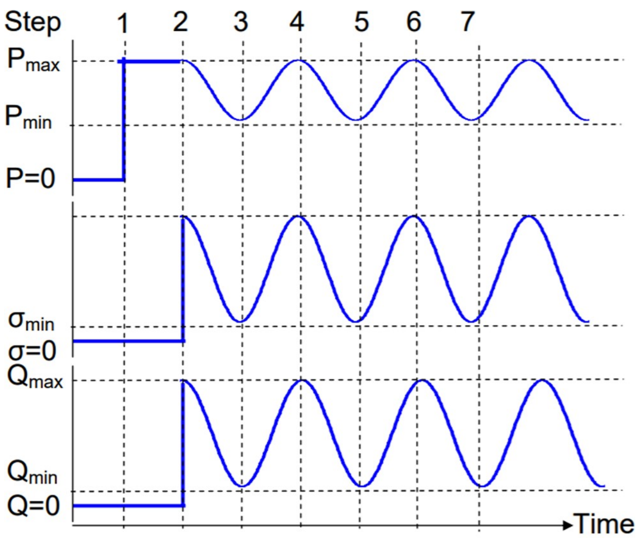

Source(s): Figure by authors

Figure 4 Seven steps of load input under out-of-phase condition of finite element analysis (FEA)

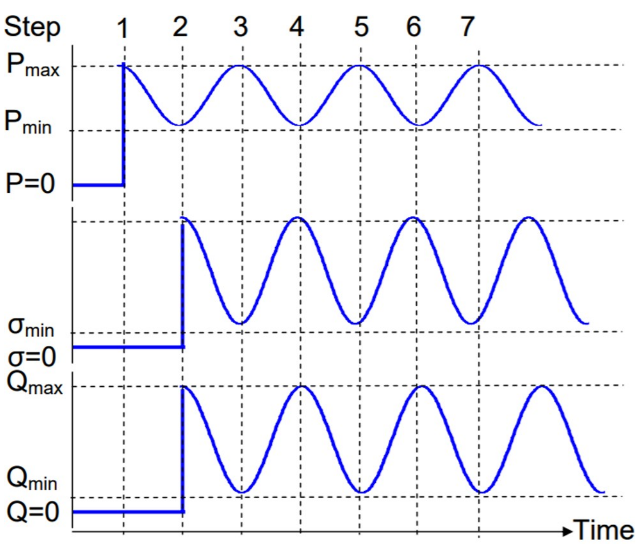

Source(s): Figure by authors

frequency of 10 Hz. The technique employed to enter the input data was varied for each case:

- For the in-phase condition, the 1st step was to apply the maximum contact load and maintain it at a constant value until reaching the 2nd step. The 2nd step was to apply the maximum-magnitude load to both the axial and tangential loads (Figure 3).
- For the out-phase, in 2nd step, the minimum magnitudes of both axial and tangential loads were applied (Figure 4).
- In the 2nd step for the other two cases (60° and 105°), both the axial and tangential loads were chosen to be related to the normal load at the specified time (Figure 5).
- After the 2nd step, a sinusoidal function is used to represent the applied loads. All input data are listed in Table 1 as obtained from (Almajali *et al.*, 2019, and Almajali, 2006).

Figure 6 shows the three applied loads (axial, normal, and tangential) against the angle for the out-of-phase test obtained from the experimental study (Almajali, 2006). It is clear that the tangential load follows the axial load, whereas the normal load does not affect the tangential load. This means that the contact load has only an impact on the magnitude of the tangential load, whereas it does not have an impact on the phase angle.

Finite element analysis comparison

Therefore, it was imperative to verify the established FEA model. The results of this study were compared with those of the Ruiz program, in which the load values were obtained at 10,000 cycles. Ruiz program is adequate tool to conduct such validation. It was used successfully in several studies such (Jutte, 2004), (Lee *et al.*, 2003) and (Eloucine, 2006). The comparison was performed only for in-phase and out-of-phase tests. The validation process considers the maximum and minimum axial load conditions. The results of this comparison for Test 2 are presented in Figures 7–10, illustrating the normalised axial stress, normalised normal stress, and normalised shear stress versus the normalised contact length x/a. These results closely align with those obtained from the step-load and Ruiz programs. By the results of many previous studies, the MSSR factor was considered to be the most influential factor in predicting material life. It is also used to predict crack initiation orientation and location. Thus, it was employed as the primary critical factor in this study. The calculation was directed along all planes with θ ranging from $-90° < \theta < +90°$, incrementing by 0.1° along the specimen, where θ is the orientation angle. Only two steps were required for the calculations: the maximum and minimum values of the stresses.

The maximum MSSR magnitude was investigated for the orientation, location, and material correlation. Table 2 displays the MSSR calculations of Test 2 for all seven required steps. The maximum MSSR magnitude was assigned to the MSSR with the greatest value of 30.42. This MSSR parameter will be investigated mainly for material fatigue life. The stress profiles computed from the FEA and the Ruiz program for test 1 (step 2) are shown in Figure 7. This figure validates that the axial, normal and shear stress curves from FEA model agree with those from the theoretical solution. For the purpose of this validation, FEA outputs are compared to the results expected by the theoretical solution under the same load conditions. The check is conducted by comparing the contact half-width, the stress profile, Hertzian peak pressure, and nominal stress from both solutions. Good agreement is clear between the results of FEA model and the theoretical solution. For instance, at x/a =0.961, the maximum values of axial stress from the FEA were approximately 986 MPa and 899 MPa from the Ruiz program. The variations in stress value and location were 8.8% and 3.9%, respectively. Figures 8–10 demonstrate all axial, normal and shear stresses in details for the same test.

Figure 5 Seven steps of load input under 60 and 105 phase degree condition of finite element analysis (FEA)

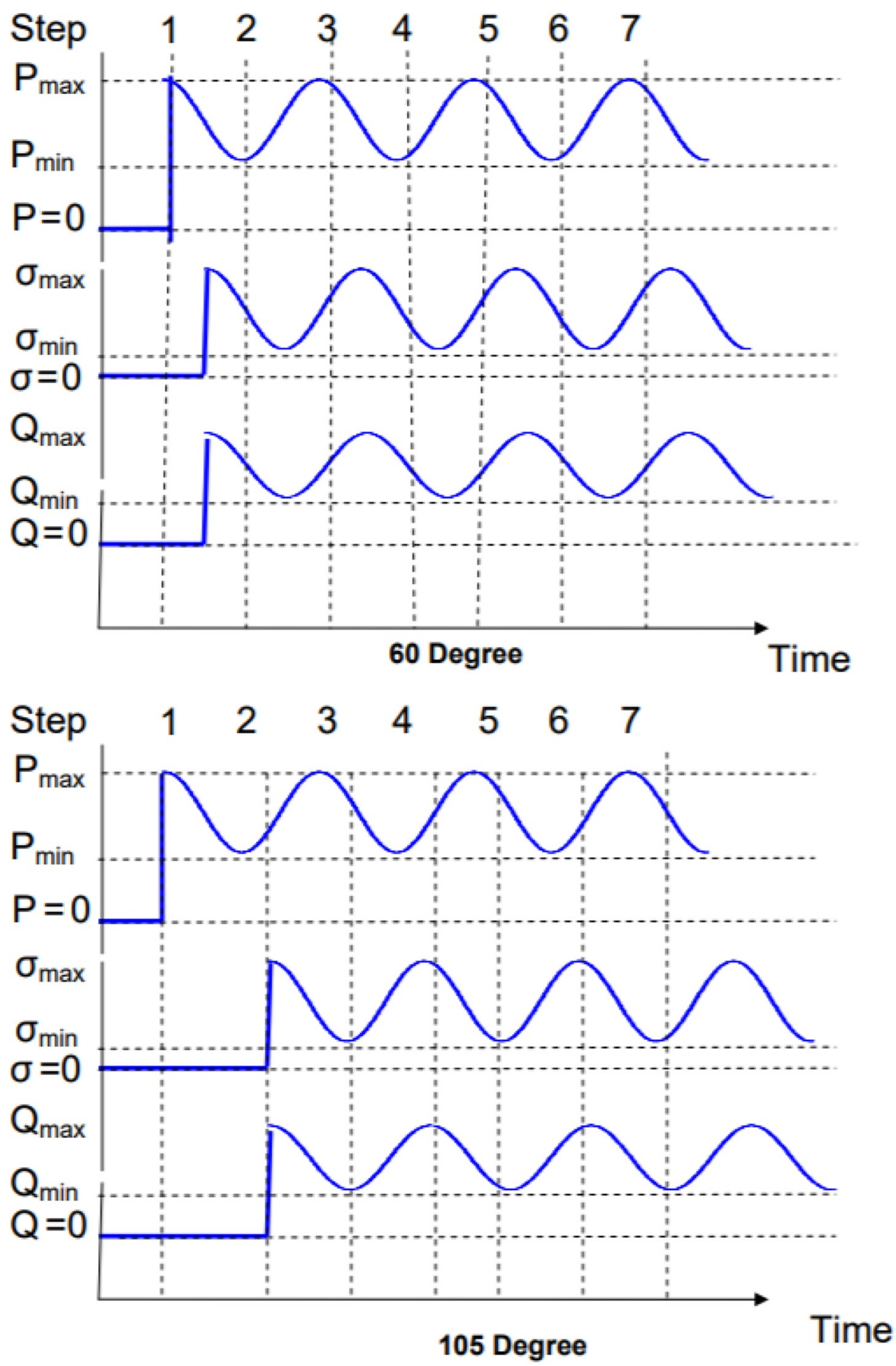

Source(s): Figure by authors

Results and discussion

In this study, an FEA model was used to determine the distribution of the required variables at the contact area, such as stress, strain, and displacement. The load conditions of the axial, contact, and tangential loads at 10,000 cycles were used as the input into the FEA (Table 1). A comparison between the results of this study and those of the Ruiz program and experimental study (Almajali, 2006) is as follows:

- For Test 1, (Almajali, 2006) investigated the contact region experimentally using a lower magnification microscope and Scanning Electron Microscope (SEM). Using FEA, the contact half-width a was calculated as 0.82 mm, while analytically it was 0.801 mm and

Table 1 Finite element analysis (FEA) load input data

Test	σ_{max} MPa	σ_{min} MPa	P_{max} MPa	P_{min} MPa	Q_{max} MPa	Q_{min} MPa	*Phase angle* °
1	564.267	56.447	36.77	73.546	3.6956	−15.43	90
2	564.267	56.427	73.546	36.77	8.0531	−13.955	0
3	172.665	470.12	73.546	36.77	1.2962	−9.4251	60
4	62.0252	548.08	73.546	36.77	7.0051	−12.355	105

Source(s): Table by authors

Figure 6 Loads vs angle for test # 2 at 10,000 cycles (out of phase condition)

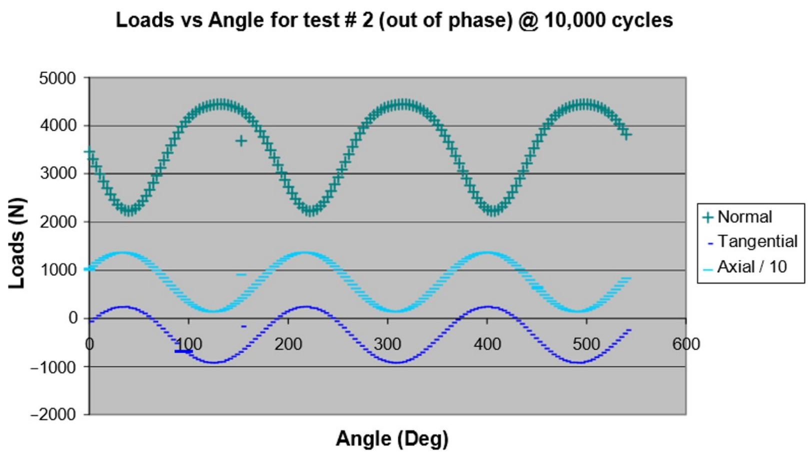

Source(s): Figure by Almajali (2006)

Figure 7 Stress profile (axial, normal and shear) for step 2 of test 1 (in-phase) from FEA and Ruiz program

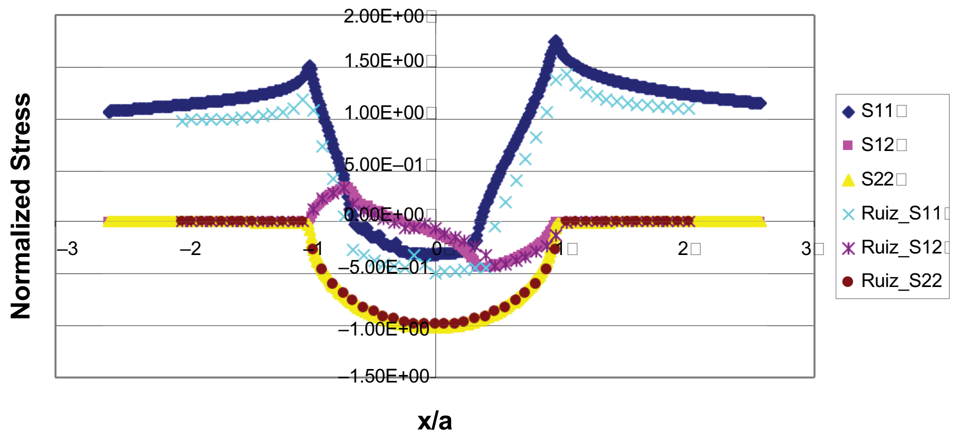

Source(s): Figure by authors

experimentally was 0.77 mm. There is a very small variation from the analytical solution, approximately 2%, and it can be assumed that the form Ruiz program is identical to the FEA calculation for all running tests. Experimentally, it was very difficult to measure the contact half-width because its length was very small, and a severe slip condition was observed at the final stage of the test (Almajali, 2006). So, different magnitudes of the contact half-width were determined with a range between 0.76 mm ∼ 0.818 m. The deviation between the numerical solution and the experiment ranged from 0.2%−7.3% which is in good agreement.

- The estimated stress profile was also very close; that is, at the ratio of x/a = 0.96 for step # 2, the maximum

Figure 8 Normalised axial load for both finite element analysis (FEA) and Ruiz program (test 2)

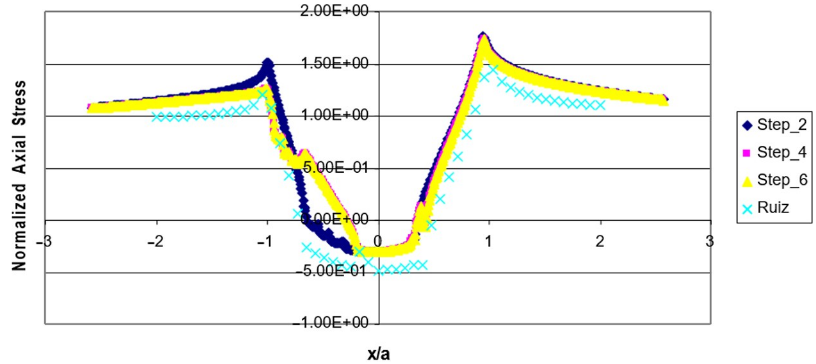

Source(s): Figure by authors

Figure 9 Normalised shear load for both finite element analysis (FEA) and Ruiz program (test 2)

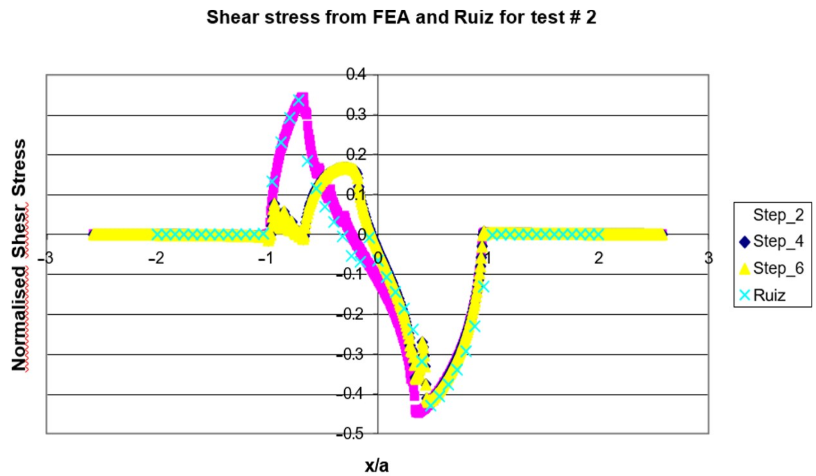

Source(s): Figure by authors

Figure 10 Normalised normal load for both finite analysis (FEA) and Ruiz program (test 2)

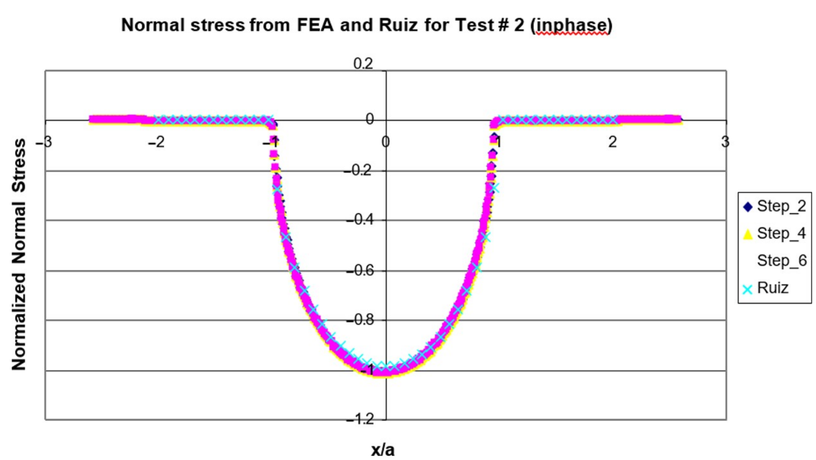

Source(s): Figure by authors

Table 2 Modified shear stress range for in-phase condition (test 2)

Between steps	MSSR	$\Delta\tau$ MPa	$\Delta\tau$crit MPa	θ Deg	σ_{max} MPa	σ_{min} MPa	x/a_{max}	x/a_{min}
2–3	30.42	394.5	408.4	40.8	414.18	29.31	1.34	0.95
3–4	30.17	388.93	402.81	40.5	406.5	29.58	1.34	0.95
4–5	30.18	389.16	402.92	40.5	406.5	29.29	1.34	0.95
5–6	30.15	388.91	402.67	40.5	405.3	29.29	1.34	0.95
6–7	30.15	389.19	402.80	40.5	405.3	28.95	1.34	0.95

Source(s): Table by authors

magnitude of the axial stress from the FEA was 986 MPa, and that from the Ruiz program was 899 MPa. The difference was approximately 8.8%, which is relatively small also.

- The Hertzian peak pressures, Po, from FEA were found to be 571 MPa and 557 MPa analytically (the variation was 2.4%).
- These results confirm that the FEA agrees with the analytical solution.

Axial stress σ_{xx}

The state of the axial stress is discussed by comparing step # 2 of the FEA results of Test 1 (out-of-phase) and Test 2 (in-phase) with those of the Ruiz program (the analytical solution), as shown in Figure 11. The conditions of the axial loads applied in the two tests were identical. Figure 11 shows Step 2 for the results of the analytical solution and FEA. The normalised axial stress, σ_{xx}, indicates that the entire axial stress within the contact region relies on both the applied loads (contact and axial) and the tangential load. Figure 11 illustrates that the maximum magnitude of the axial stress for test 1 (out-of-phase) was determined to be 837 MPa at an x/a ratio equal to 0.985 in the FEA result and 740 MPa at x/a = 1.04 in the Ruiz program result. For the in-phase condition (Test 2), the maximum magnitude of the axial stress was computed as 994 MPa at x/a = 0.940 using FEA, and 807 MPa at x/a = 1.04 using the Ruiz program.

Hence, the following can be observed from this figure:

- The maximum stress for Test 1 computed from the Ruiz program deviated by 8% from that in Test 2, even though the location was the same (x/a = 1.04). The stress concentration factor is typically calculated as the ratio between the maximum applied stress and nominal stress. These values were 1.311 and 1.43 for tests 1 and 2. The deviation is also approximately 8%. It can be observed that the axial stress and stress concentration factor for test 1 were lower than those for test 2.
- Regarding the results of FEA, the maximum value of σ_{xx} for in-phase is 994 MPa, which is more than the out-of-phase value (837 MPa) with a deviation of approximately 16%. The locations also differed by approximately 5%. The stress concentration factor for test 1 (out-of-phase) was 1.483, and for test 1 (in-phase), it was 1.762, with a deviation of 16%.
- Comparing the Ruiz program with the FEA, the differences for the in-phase condition are 12% in the maximum value of σ_{xx} with 5% in location and for the out-of-phase condition 19% in maximum σ_{xx} with 10% in location. From the above results, it can be seen that the results for the out-of-phase condition are closer to those of the analytical solution. However, the maximum magnitude of σ_{xx} for the out-of-phase test was less than that for the in-phase test. This, in turn, results in a lower stress concentration factor in σ_{xx} for the out-of-phase condition, which indicates that the fatigue life of the material will increase compared with the in-phase condition.

Figure 11 Normalised axial stress for step 2 of tests 1 and 2

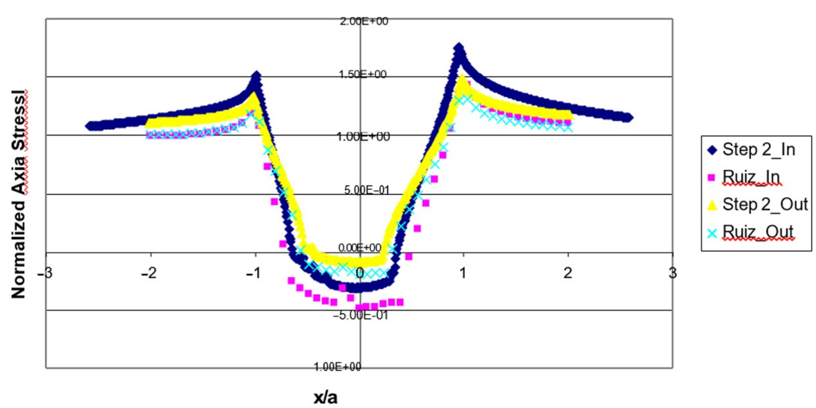

Source(s): Figure by authors

World Journal of Engineering
Volume 23 · Number 2 · 2026 · 378–393

Figure 12 Normalised normal stress for step 2 of tests 1 and 2

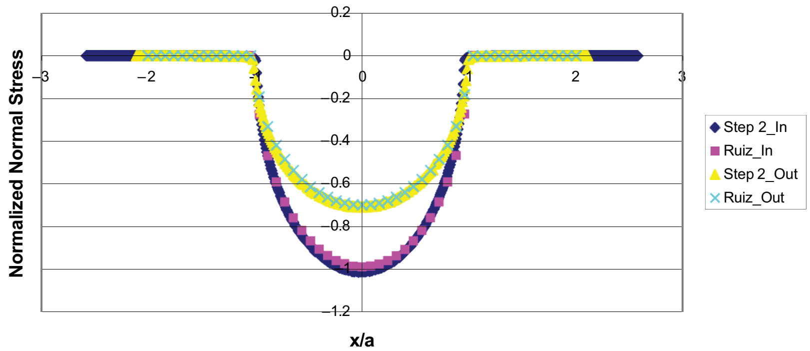

Source(s): Figure by authors

Normal stress σ_{yy}

The same conditions employed in the previous section for the distribution of the normal stress σ_{yy} are utilised here, as illustrated in Figure 12. The Figure clearly shows a remarkable agreement between the Ruiz program and FEA, with both methods producing nearly identical outputs. However, a significant disparity in the results emerges when the phase-angle condition is considered. For the in-phase condition, the maximum σ_{yy} was approximately 560 MPa according to the Ruiz program and 570 MPa according to the FEA. In contrast, for the out-of-phase condition, these values are 395 MPa (Ruiz) and 400 MPa (FEA). Notably, there was no discernible difference between the FEA and Ruiz program outputs for each test; however, a substantial difference was observed between the in-phase and out-of-phase conditions, leading to a deviation of approximately 30%. This is because, when the case is in the in-phase condition, both the axial load and contact load are at their maximum or minimum magnitudes simultaneously. However, when the case is out-of-phase if the axial stress is at its maximum value, the contact load is at its minimum value, and vice versa.

Shear stress σ_{xy}

For shear stress analysis, a distinct approach was employed to identify the maximum load conditions. In test 2 (in phase), step 2 considers the maximum σ_{yy} and maximum. For test 2 (out-of-phase), step 2 considered the maximum σ_{xx} and minimum σ_{yy}, whereas step 3 involved the minimum σ_{xx} and maximum σ_{yy}. These conditions are illustrated in Figure 13. Notably, Figure 13 indicates that step 2 for the out-of-phase condition aligns more closely with step 2 for the in-phase condition than step 3. Step 3 behaved differently, representing the maximum axial stress (σ_{xx}) for both conditions, exhibiting nearly identical shear stress levels. This observation reveals that the maximum magnitude of the axial stress σ_{xx} represents the critical load condition in this study. As the maximum axial load is considered under the primary load condition, this condition is satisfied in steps (2, 4 and 6) for the out-of-phase condition, as depicted in Figures 14–16. The maximum axial, shear, and normal stresses for these steps are almost identical at the same location (x/a). Thus, the sequence of applied loads has no impact; only the magnitude of the applied load matters, a conclusion that is

Figure 13 Shear stress for test 2 (step 2) and test 1 (steps 2 and 3)

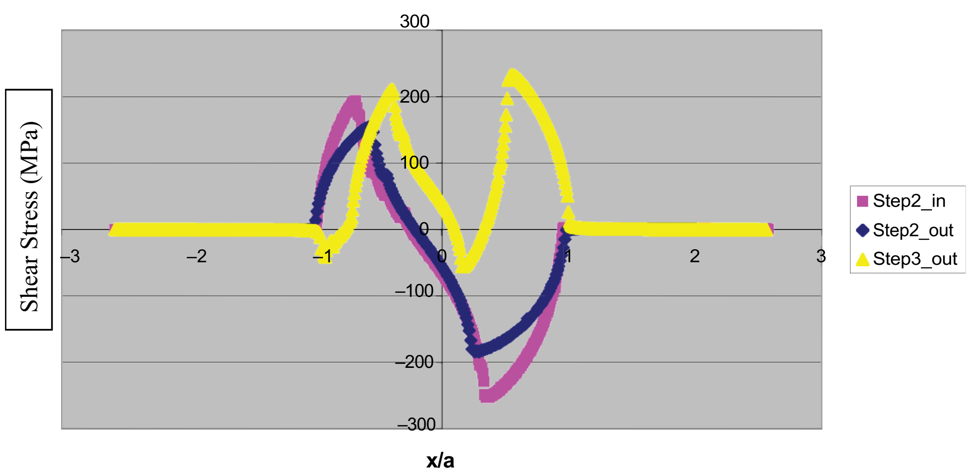

Source(s): Figure by authors

Figure 14 Axial stress for test 1 (steps 2, 4 and 6) (out of phase)

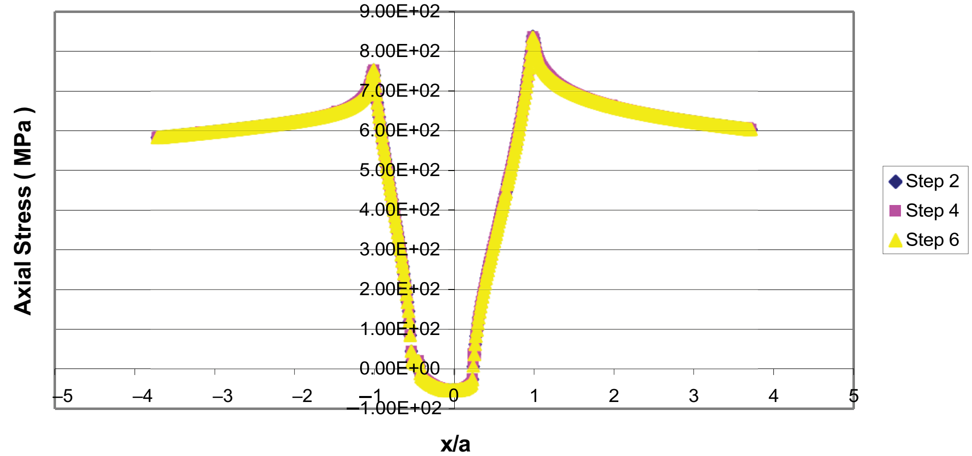

Source(s): Figure by authors

Figure 15 Shear stress for test 1 (steps 2, 4 and 6) (out of phase)

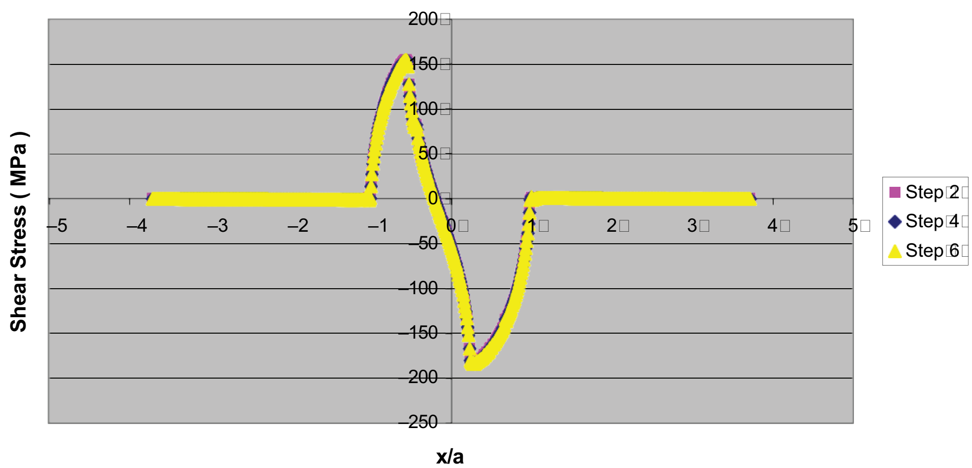

Source(s): Figure by authors

consistent for both the maximum and minimum load conditions.

Modified shear stress range calculation

As indicated earlier, the maximum load condition was identified as the maximum axial load for both the in- and out-of-phase conditions. The out-of-phase stress output demonstrated a closer alignment with the analytical solution than the in-phase stress. In addition, the stress concentration factor at the same axial stress for the out-of-phase condition was lower than that for the in-phase condition. To validate the FEA model, the results were compared with those obtained from the analytical Ruiz solution and experimental results (Almajali, 2006). The FEA considered various parameters, including the in-phase and out-of-phase conditions, load conditions and stress distribution. The examination of parameters, including the MSSR, effective stress, stress range, and tangential load range, aimed to determine their effects on the material life and crack initiation conditions in terms of orientation and location. The MSSR, the most influential factor in predicting life and crack mechanisms, was highly active in defining the crack mechanism and was effective for in-phase fatigue life. However, under the same axial load conditions for the out-of-phase condition, the MSSR was slightly higher than that for the in-phase condition, resulting in a longer fatigue life. This discrepancy arises because the MSSR depends on three parameters: the maximum axial load, critical shear stress range and arbitrary constant. Therefore, when studying fretting fatigue from a phase angle, MSSR must be evaluated using different approaches, including alterations in arbitrary constants.

The calculation of the MSSR requires only two steps of load application (the maximum and minimum values). Therefore, it is necessary to compute the MSSR between different step pairs of the seven steps, which results in a total of five MSSR values, as shown in Table 2. The maximum MSSR value is considered.

Figure 16 Normal stress for test 1 (steps 2, 4 and 6)

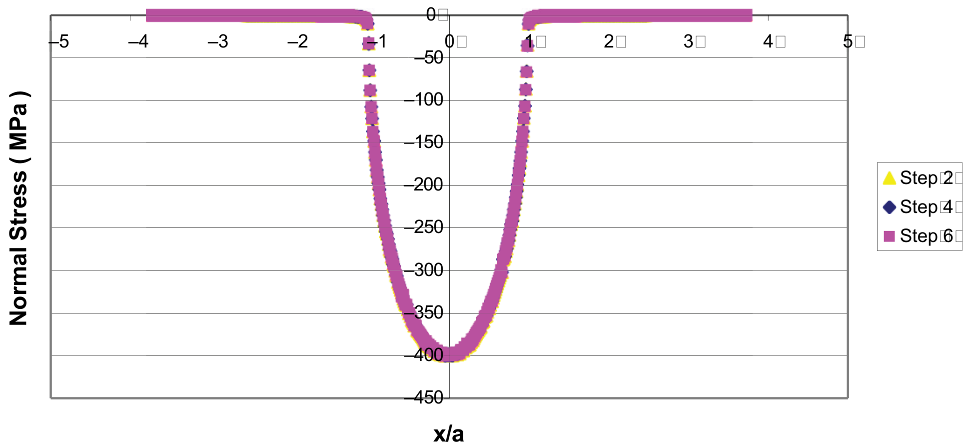

Source(s): Figure by authors

Figure 17 Max MSSR vs axial stress for in-phase and out-phase tests

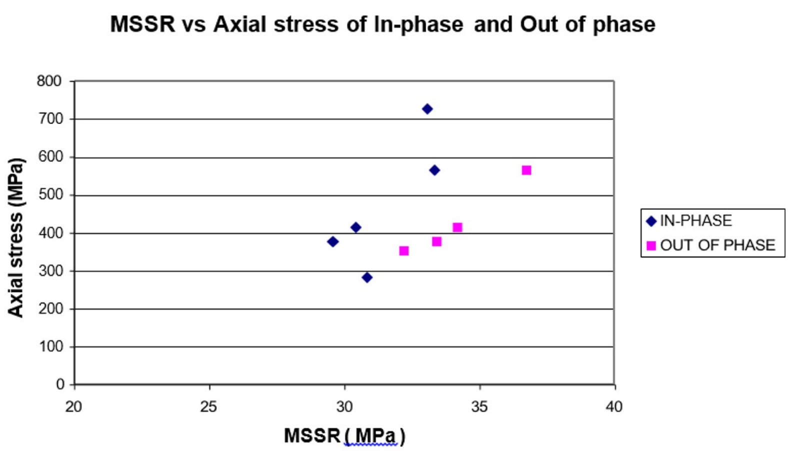

Source(s): Figure by authors

The data from Table 2 are plotted in Figure 17, which shows the variation in the MSSR with the axial load for both in-phase and out-of-phase conditions. The MSSR for the out-of-phase phase is higher than that of the in-phase. This is because the MSSR depends primarily on the combination of the axial and shear stresses. It can also be concluded that there is a proportional relationship between the axial load and MSSR. Figure 18, on the other hand, shows the relationship between the phase angle and the maximum value of the MSSR. This Figure shows that the MSSR increased with an increase in the phase angle from 0° (in-phase) to 90° (out-of-phase). Then, the MSSR started to decrease, which indicates that the maximum value of MSSR was determined in the out-of-phase condition, and the minimum value was determined in the in-phase condition.

Crack initiation and orientation

The contact half-width depends primarily on the contact load, which is considered a variable in this study. The variation in contact load resulted in two extreme values (minimum and maximum). The location of the crack initiation resulting from MSSR was then divided by both the maximum and minimum values. This, in turn, specifies two crack initiation locations (Table 3). This table shows the two values of the crack initiation location in the last two columns. The maximum and minimum values of crack initiation for the in-phase condition are x/a = 1.373 and x/a = 0.945, respectively. These values for the out-of-phase condition are x/a = 0.99 and x/a = 0.683. Because there are two values of the location of the crack initiation, there is an argument about which one of them should be considered as the actual location of the crack initiation. From the theoretical background, for the in-phase condition, all loads (axial, tangential and normal) were at their maximum values (Figure 3). Therefore, the value of the contact half-width, a, is the maximum. Therefore, the crack location of the MSSR should be divided by the maximum value of the contact half-width. This results in a minimum value of x/a of 0.95. However, for the out-of-phase condition, the maximum load

Figure 18 Max MSSR vs phase angle

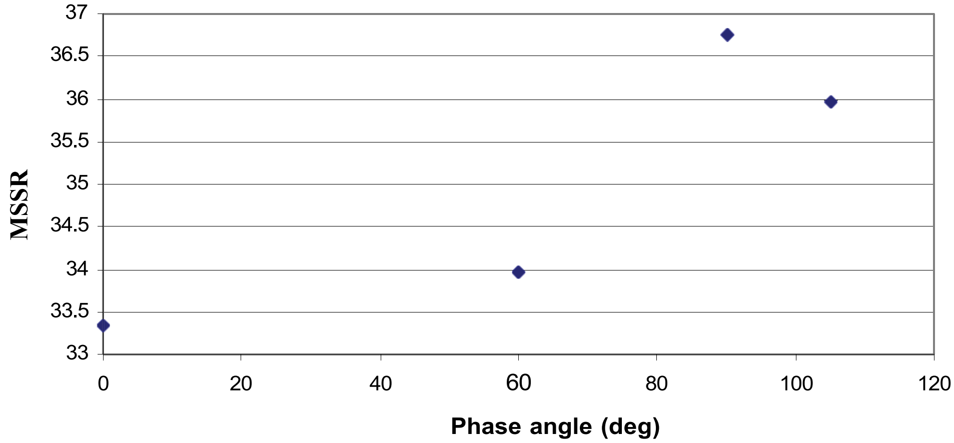

Source(s): Figure by authors

Table 3 Max MSSR calculation for in-phase and out-of-phase tests

Test	MSSR	$\Delta\tau$ MPa	$\Delta\tau$crit MPa	Θ Deg	R$\Delta\tau$	σ_{max} MPa	σ_{min} MPa	Depth mm	x/a_{max}	x/a_{min}
In-phase	*33.347*	482.776	491.19	42.8	0.0309	497.27	16.508	0.1114	1.3736	0.9535
Ou-of-phase	*36.748*	752.294	540.04	60.5	−1.2091	663.5	230.8	0.1029	0.9845	0.6834

Source(s): Table by authors

Figure 19 Crack initiation orientations for test # 1 (in-phase)

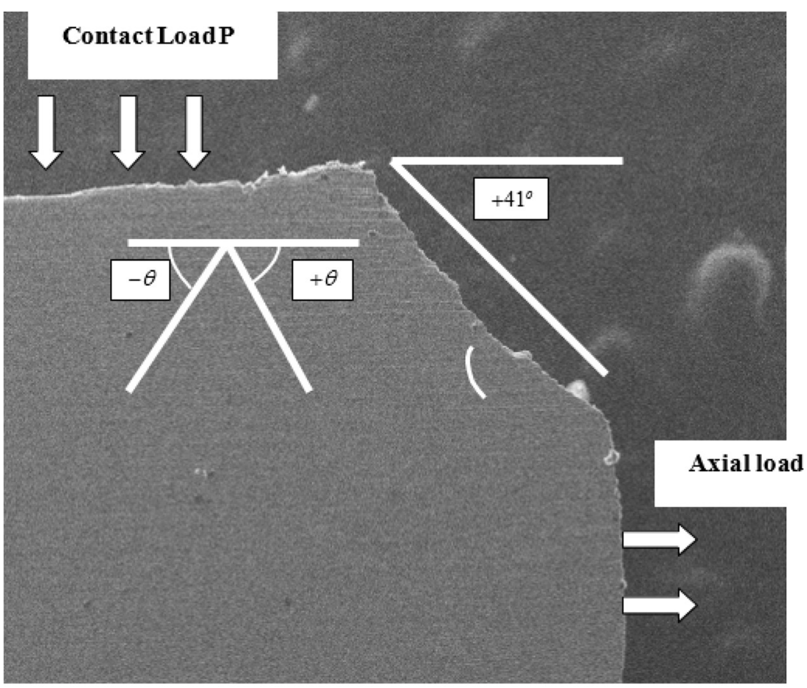

Source(s): Figure by Almajali (2006)

condition occurred at the minimum value of the contact load (Figure 4). Alternatively, the result of the location of the crack from MSSR is divided by the minimum value of the contact half-width. This resulted in the maximum value of x/a and provided the location at x/a = 0.99.

The values of the location of the crack obtained above were in very good agreement with the analytical solution. For instance; the value for test # 1 (in-phase) is 0.9535 and for test # 2 (out-of-phase) is 0.9845. The deviations of these values were 4.65% and 1.55%, respectively. These values are also very close to the results of an experimental study by (Almajali, 2006). Table 3 also lists the crack-initiation orientation for the tests conducted. The crack orientation angle under the in-phase condition was approximately 42.8°. This value is in very good agreement with the previous studies (– 45° or + 45°) ±15° and the experimental study of Almajali (Almajali, 2006) as shown in Figure 19, with the crack orientation of 41°, which gives a deviation of 4.2% from this study. In contrast, the orientation crack angle for the out-of-phase condition was approximately 60.5°. This value is also very close to the experimental study (Almajali, 2006) as shown in Figure 20 (63°), and the deviation was approximately 3.9%.

Conclusion

An FEA model was developed to predict the fatigue life and crack mechanisms of materials in contact using the ABAQUS commercial software. To avoid gross slip, a maximum normal load was applied in the initial step. In Step 2, the maximum axial and tangential loads, along with the tangential load, were applied. The frequency remained constant across all applied loads, spanning seven steps. The friction coefficient, established as 0.5, from prior studies, was maintained. A comparison between the FEA and Ruiz program was conducted to validate the FEA model, with the maximum axial load identified as the critical load condition. FEA meticulously considered all pertinent parameters. The input data for the MSSR were extracted from the FEA outputs, assuming it to be the most influential factor in predicting material life and crack details. Other parameters, including the axial stress range, effective stress, and tangential load range were also investigated.

Across all the tests with phase differences, crack initiation consistently occurred near the trailing edge of the contact area, approximately at x/a ≈ +1. The highest Q/P ratio magnitude was observed in the in-phase condition and the lowest in the out-of-phase condition. This indicates that the out-of-phase condition has less friction than the in-phase condition which results in increasing the fatigue life. Additionally, for the out-of-phase condition, both the maximum axial and tangential load (Q) ranges were lower than those in the in-phase condition. The MSSR exhibited a 10% higher value in the out-of-phase condition compared to the in-phase condition. It was deduced that MSSR significantly influenced the prediction of crack initiation, details, and material life. The crack initiation location was determined to be x/a = 0.95 for the in-phase condition and 0.98 for the out-of-phase condition, indicating a 145% increase in fatigue life for the out-of-phase condition compared to that in the in-phase condition. This result of the life increase of the out pf phase is in a good agreement with the previous works conducted by (Gailliegue *et al.*, 2020) and (Wang *et al.*, 2023). This study focused on numerically investigating the effect of the phase difference between axial and contact loads on fretting fatigue.

It can be concluded that the MSSR is an effective parameter for predicting the details of crack initiation. In conclusion, the

Figure 20 Crack initiation orientations for test # 2 (out of phase)

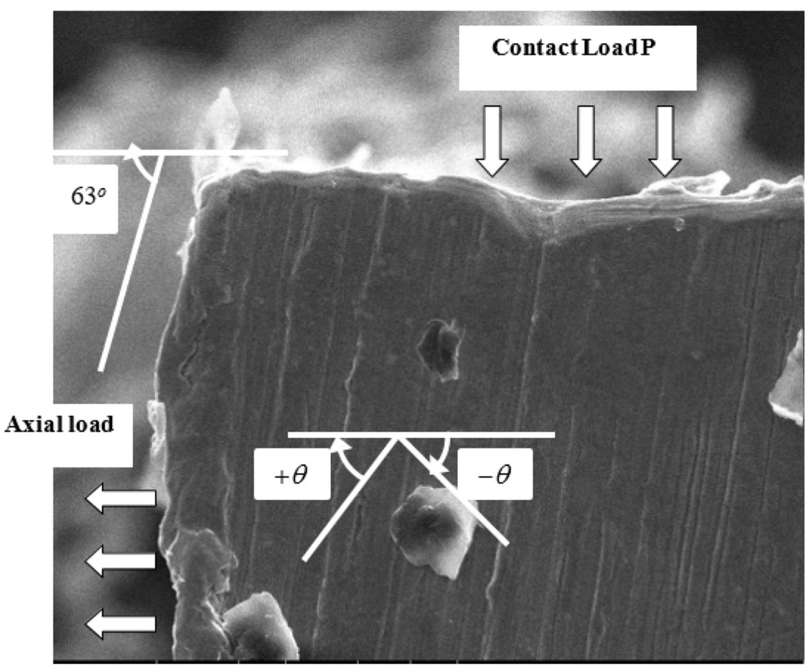

Source(s): Figure by Almajali (2006)

maximum MSSR value was obtained between two different steps of each test. Although the frequency was maintained constant at 10 Hz, the two steps under in-phase or out-of-phase conditions differed from one test to another. At the same axial load, the MSSR values were higher under the out-of-phase condition. MSSR was very effective in predicting both the location and orientation of crack initiation. In real life, the frequencies of the axial and contact loads are high; however, in this study, it was assumed to be 10 Hz because there was a limitation on the test machine during the experimental study (Hu *et al.*, 2019). Additionally, this fretting fatigue phenomenon occurs mainly in the turbine section of aircraft engines and corrosion environments, which means that elevated temperatures and environmental corrosion should be considered, which was not considered in this study. The study was also conducted on one material, namely, titanium alloy, and it is preferable to employ different materials.

The developed model can help designers predict how the structure will behave under different types of stresses to determine the design flaws. They can use the results of different case scenarios to make the essential modifications to the desired prototypes. The designers can run simulations under different conditions to evaluate how the structure of the product will behave under applied different loads. They can be able to modify to meet the standard product and safety precautions. This model can allow designers to examine, predict, and optimise the prototype before production.

References

Abbasi, F., Majzoobi, G. and Mendiguren, J. (2020), "A review of the effects of cyclic contact loading on fretting fatigue behavior", *Advances in Mechanical Engineering*, Vol. 12 No. 9, doi: 10.1177/1687814020957175.

Ahmad, S., Badshah, S., Rahimian Koloor, S.S., Amjad, M., Jan, S. and Tamin, M.N. (2024), "Cumulative fretting fatigue damage model for steel wire ropes", *Fatigue & Fracture of Engineering Materials & Structures*, Vol. 47 No. 5, pp. 1656-1676, doi: 10.1111/ffe.14264.

Almajali, M. (2006), "Effects of the phase difference between axial and contact loads on fretting fatigue behavior of titanium alloy", Thesis, Air Force Institute of Technology, Wright-Patterson Air Force Base, OH.

Almajali, M., Mall, S. and Almahadin, A. (2019), "Fretting fatigue behavior under phase difference between axial and contact loads", *Scholar Journal of Applied Sciences and Research*, Vol. 2 No. 5, pp. 16-22, doi: 10.3619/SJASR.1000230.

Chan, K. and Lee, Y. (1988), "Ruiz program", South West Research Institute, Personal Communication.

Chaouch, M., Baltach, A. and Benhamena, A. (2022), "Numerical analysis of geometrical parameters effect on contact zone under fretting fatigue loading", *Advances in Materials Science*, Vol. 22 No. 4, pp. 5-20, doi: 10.2478/adms-2022-0015.

Chen, H., Wei, D., Wang, Y. and Shi, L. (2018), "Experimental and numerical study of fretting fatigue in dovetail assembly using a total life prediction model", *Engineering Fracture Mechanics*, Vol. 205, doi: 10.1016/j.engfracmech.2018.08.001.

Dowson, D., Taylor, C., Godet, M., Berthe, D. and Ed, S (1988), *Mechanical Engineering Publications*, Elsevier, Amsterdam, pp. 92-103.

Eloucine, M. (2006), "Fretting fatigue behavior of nickel alloy in-100", Thesis, Air Force Institute of Technology, Wright-Patterson Air Force Base, OH.

Gailliegue, T., Doca, T., Araújo, J. and Ferreira, J. (2020), "Fretting life of the Al7050-T7451 under out-of-phase loads: numerical and experimental analysis", *Theoretical and Applied Fracture Mechanics*, Vol. 106 No. 2, p. 102492, doi: 10.1016/j.tafmec.2020.102492.

Gonggui, Y., Jun, H., Van, H. and Ping, H. (2021), "A new method for measuring stress inside movable element in contact", *Tribology Letters*, Vol. 69, doi: 10.1007/s11249-021-01535-6.

Hills, D. and Nowell, D. (1994), "*Mechanics of Fretting Fatigue*", Springer Science and Business Media, Cham, ISB: 0792328663, 9780792328667.

Hintikka, J. (2016), "Fretting induced friction, wear and fatigue in quenched and tempered steel", Tampere University of Technology. Vol. 1392.

Hu, C., Wei, D., Wang, Y. and Shi, L. (2019), "Experimental and numerical study of fretting fatigue in dovetail assembly using a total life prediction model", *Engineering Fracture Mechanics*, Vol. 205, pp. 301-318, doi: 10.1016/j.engfracmech.2018.08.001.

Huang, Z., Zhang, Z., Teng, Z., Khan, M., Wang, Q. and Wang, J. (2019), "Effect of fretting damage on characteristics of high strength bearing steel up to very high cycle fatigue", *Engineering Fracture Mechanics*, Vol. 217, p. 106526, doi: 10.1016/j.engfracmech.2019.106526.

Iyer, K. and Mall, S. (2000), "Effects of cyclic frequency and contact pressure on fretting fatigue under two-level block loading", *Fatigue & Fracture of Engineering Materials & Structures*, Vol. 23 No. 4, pp. 335-346, doi: 10.1046/j.1460-2695.2000.00288.x.

Jutte, A. (2004), "Effect of a variable contact load on fretting fatigue behavior of Ti- 6Al-4V", Thesis, Air Force Institute of Technology, Wright-Patterson Air Force Base, OH.

Kadiric, R., Xiao, S., Zhou, B. and Ioannides, E. (2003), "A numerical study of the contact mechanics and subsurface stress effects experienced over a range of machined surface coatings in rough surface contacts", *Journal of Tribology*, Vol. 125 No. 4, pp. 720-730, doi: 10.1115/1.1574520.

Lee, H., Jin, O. and Mall, S. (2003), "Fretting fatigue behaviour of shot-peened Ti-6Al-4V at room and elevated temperature", *Fatigue and Fracture of Engineering Material and Structure*, Vol. 26, pp. 767-778, doi: 10.1046/j.1460-2695.2003.00677.

Lietch, L. (2004), "Fretting fatigue behavior of the titanium alloy Ti-6Al-4V under seawater conditions", Thesis, Air Force Institute of Technology, Wright-Patterson Air Force Base, OH.

Lykins, C., Mall, S. and Jain, V. (2001), "A shear stress based parameter for fretting fatigue crack initiation", *Fatigue & Fracture of Engineering Materials & Structures*, Vol. 24 No. 7, pp. 461-473, doi: 10.1046/j.1460-2695.2001.00412.x.

Nowell, D., Dini, D. and Hills, D. (2006), "Recent developments in the understanding of fretting fatigue", *Engineering Fracture Mechanics*, Vol. 73 No. 2, pp. 207-222, doi: 10.1016/j.engfracmech.2005.01.013.

Sangral, S. and Jayaprakash, M. (2022), "Evaluating the effect of contact pad geometry on the fretting fatigue behavior of titanium alloy by experimental and finite element analysis", *Journal of Failure Analysis and Prevention*, Vol. 22 No. 2, pp. 773-784, doi: 10.1007/s11668-022-01369-x.

Toshikazu, A., Mitsuo, N., Hisao, F. and Akihiro, S. (2004), "Fatigue, fretting fatigue and corrosion characteristics of biocompatible beta type titanium alloy conducted with various Thermo mechanical treatments", *Materials Transactions*, Vol. 45 No. 5, pp. 1540-1548, doi: 10.2320/matertrans.45.1540.

Wang, C., Pereira, K., Wang, D., Zinovev, A., Terentyev, D. and Abdel Wahab, M. (2023), "Fretting fatigue crack propagation under out-of-phase loading conditions using extended maximum tangential stress criterion", *Tribology International*, Vol. 187, p. 108738, doi: 10.1016/j.triboint.2023.108738.

Waterhouse, R. and Dutta, M. (1973), "The fretting fatigue of titanium and some titanium alloys in a corrosive environment", *Wear*, Vol. 25 No. 2, pp. 171-175, doi: 10.1016/0043-1648(73)90069-0.

Xiaohua, Z., Kaifa, F., Daoxin, L. and Junfeng, X. (2021), "Numerical study on fretting fatigue crack initiation behaviors of Ti-6Al-4V alloy", *Journal of Failure Analysis and Prevention*, Vol. 21, doi: 10.1007/s11668-021-01164-0.

Xin, Q. (2013), "Durability and reliability in diesel engine system design", *Diesel Engine System Design*, pp. 113–202, doi: 10.1533/9780857090836.1.113.

Zehsaz, M. and Shahriary, P. (2013), "The effects of friction coefficient and interference on the fretting fatigue strength of railway axle assembly", *UPB Scientific Bulletin*, Vol. 75 No. 4, pp. 1454-2358.

Zhibo, G., Pei, Y., Huiqing, G., Yifan, S., Jiao, L. and Xibin, W. (2023), "The torsional fretting wear behavior of titanium alloy", *In Book: New Materials, Machinery and Vehicle Engineering License CC by-NC 4.0*, IOS Press, Amsterdam, doi: 10.3233/ATDE230120.

Zou, L., Zeng, D., Tian, X., Jiang, G., Dong, Y., Zhao, H. and Lu, L. (2024), "Experimental and numerical study on the multi-site fretting fatigue crack initiation of press-fitted axles", *Fatigue and Fracture of Engineering Material and Structure*, Vol. 47 No. 2, pp. 473-490, doi: 10.1111/ffe.1.

Further reading

Wang, Y., Yan, Z. and Wu, Y. (2024), "Numerical simulation of fretting fatigue damage evolution of cable wires considering corrosion and wear effects", *CMES, Computer Modeling in Engineering & Sciences*, Vol. 136 No. 2, pp. 1339-1370, doi: 10.32604/cmes.2023.025830.

Corresponding author

Mohammad Almajali can be contacted at: malmajali@ra.ac.ae